JOURNAL OF AIRCRAFT
Vol. 38, No. 2, March–April 2001

Analytical-Experimental Correlation for a Stiffened Composite Panel Loaded in Axial Compression

Oung Park,* Raphael T. Haftka,† and Bhavani V. Sankar‡
University of Florida, Gainesville, Florida 32611-6250
James H. Starnes, Jr.§
NASA Langley Research Center, Hampton, Virginia 23681
and
Somanath Nagendra¶
General Electric Corporate Research & Development Center, Schenectady, New York 12309

A combined analytical and experimental study of a blade-stiffened composite panel subjected to axial compression was conducted. The study first examined the effects of the differences between a simple model used to design the panel and the actual experimental conditions. It was found that the large imperfection used in the design process compensated for the simplifying assumptions of the design model, and the experimental failure load was only 10% higher than the design load. Next, finite element analyses were performed in order to correlate analytical and experimental results. The buckling loads from finite element analyses agreed well with the experimental failure loads. However, substantial differences were found in the out-of-plane displacements of the panel. Finite element simulations of nonuniform load introduction with general contact definitions improved correlation between the measured and predicted out-of-plane deformations.

Introduction

STIFFENED, laminated composite panels have been considered for use in weight-sensitive structures such as aircraft and missile structural components, where high strength-to-weight and stiffness-to-weight ratios are required. High strength and in-plane stiffness properties of composite materials result in thin sections that are critical in buckling. Among the several configurations commonly used for stiffened panels, blade-stiffened panels have simple geometric configurations with good structural efficiency, which makes them a popular structural concept. Buckling loads and the sensitivity of the response to initial imperfections are often expensive to calculate with general finite element models. Consequently, the optimization of stiffened panels often employs simplified models that are exact only for idealized geometries, loading conditions, and boundary conditions (e.g., PASCO[1] or PANDA2[2]).

Nagendra et al.[3] studied the optimum design of blade-stiffened panels with cutouts subjected to buckling and strain constraints. They used the panel analysis and sizing code (PASCO[1]), based on a linked plate model, for the buckling analysis and structural optimization with continuous-thickness design variables and the engineering analysis language (EAL[4]) finite element analysis code for calculating strains and their derivatives with respect to the design variables. Later, the optimally designed panels with and without centrally located holes were tested, and analytical and experimental results were compared.[5] Nagendra et al.[6] extended the optimum design study of blade-stiffened panels using PASCO for analysis and a genetic algorithm (GA) for the optimization of panel laminate stacking sequences. Several designs obtained using GA optimization were about 8% lower in weight than designs previously obtained in Ref. 3 using a continuous optimization procedure.

Recently, three of the panels designed by Nagendra et al.[6] were fabricated and tested by the Structural Mechanics Branch at NASA Langley Research Center. The experimental failure loads differed by a maximum of approximately 10% from the design load. However, there were significant differences in loading and boundary conditions between the design conditions and the test conditions.

One objective of the present paper is to assess the effectiveness of the simplified PASCO model originally used to design the panel. A second objective is to correlate analytical and experimental results.

Stiffened Panel Definition

The panel designated as the baseline design corresponds to the ninth row in Table 7 of Ref. 6. This panel, designated as GA2461 (referring to the design weight of 24.61 lb), is 30 in. long and 32 in. wide, with four equally spaced blade stiffeners (see Fig. 1). Two other designs from Ref. 6 were also tested in the same series of tests with similar failure loads. This paper is focused on the GA2461 panel, with only occasional references to the other two panels. The laminates used for the GA2461 baseline design in Ref. 6 for the skin, stiffener blade, and stiffener flange are balanced, symmetric laminates consisting of 0 deg, ±45 deg, and 90 deg plies. The skin has 40 plies with a stacking sequence of $[\pm 45/90_4/\pm 45_3/90_2/\pm 45_3]_s$, and the stiffener flange and blade have identical stacking sequences of $[\pm 45_2/(\pm 45/0_4)_2/90_2/0_4/(\pm 45/0_2)_2/0_2/\pm 45]_s$, with a total of 68 plies. Properties of the Hercules, Inc., AS4/3502 graphite epoxy material used in Ref. 6 are given in Table 1.

The baseline panel was designed to support an axial load N_x of 20,000 lb/in. In addition, to account for off design conditions, imperfections, and modeling inaccuracies, a shear load ($N_{xy} = 5000$ lb/in.) and a longitudinal bow-type geometric imperfection (3% of the panel length) were added to the design requirements. The baseline design panel was assumed to be simply supported along the four edges, which is the only boundary condition that can be accurately modeled using PASCO.

Presented as Paper 98-1993 at the AIAA/ASME/ASCE/AHS/ASC 39th Structures, Structural Dynamics, and Materials Conference, Long Beach, CA, 20–23 April 1998; received 25 April 2000; revision received 8 November 2000; accepted for publication 27 November 2000. This material is declared a work of the U.S. Government and is not subject to copyright protection in the United States.

*Research Assistant, Department of Aerospace Engineering, Mechanics and Engineering Science; currently at Lexel Engineering, Flint, Michigan. Student Member AIAA.

†Distinguished Professor, Department of Aerospace Engineering, Mechanics and Engineering Science. Fellow AIAA.

‡Professor, Department of Aerospace Engineering, Machanics and Engineering Science. Associate Fellow AIAA.

§Senior Engineer for Structures and Materials. Fellow AIAA.

¶Mechanical Engineer, MDMP, Engineering Mechanics Laboratory. Associate Fellow AIAA.

Table 1 Hercules Inc. AS4/3502 graphite–epoxy lamina material properties

Young's modulus (longitudinal)	$E_1 = 18.50 \times 10^6$ psi
Young's modulus (transverse)	$E_2 = 1.64 \times 10^6$ psi
Shear modulus	$G_{12} = 0.87 \times 10^6$ psi
Major Poisson ratio	$\nu_{12} = 0.3$
Density	$\rho = 0.057$ lb in.$^{-3}$
Ply thickness	$t_{ply} = 0.0052$ in.

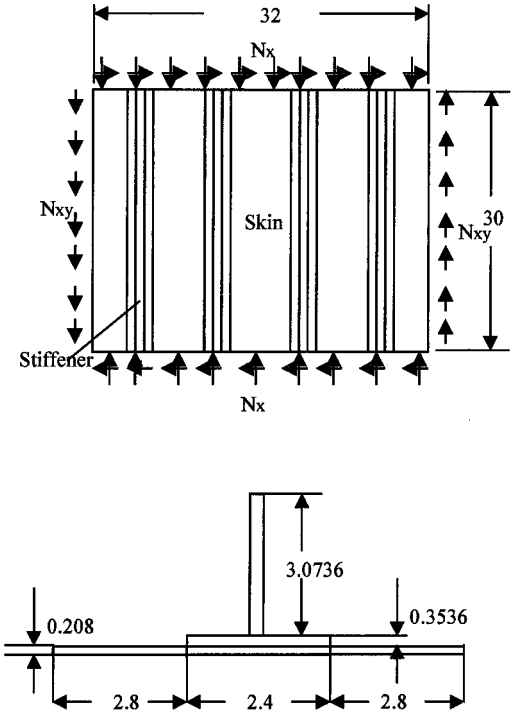

Fig. 1 Blade-stiffened panel with four equally spaced stiffeners under compression and shear loads. All dimensions are in inches.

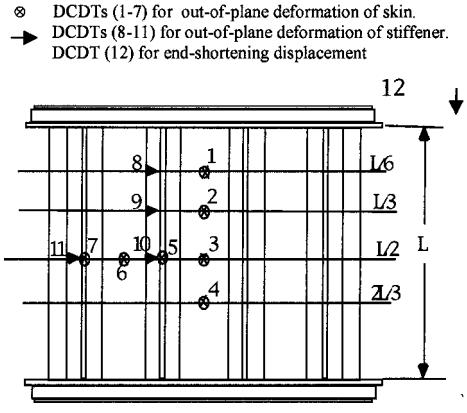

Fig. 2 Layout of the displacement measurement instrumentation (DCDTs) for the test panel.

Test Specimen and Test Procedures

The test specimens were fabricated using Hercules, Inc., AS4/3502 unidirectional graphite–epoxy preimpregnated tape material. The skin (32 × 32 in.) and stiffeners were cured separately in an autoclave. The stiffeners were machined to a length of 32 in., then bonded to the skin with FM-300 film adhesive. The panel edges perpendicular to the stiffeners were potted with an aluminum-filled epoxy resin to prevent end failure. The length of the potted area was 1 in. on each end. Thus, the effective length of the test specimen was reduced to 30 in.

The test specimen was loaded in compression using a 1,000,000-lb-capacity hydraulic testing machine. The specimen was flat-end tested without lateral edge supports, and no deliberate geometric imperfection was introduced. Electrical resistance strain gauges were used to monitor the strains and direct current differential transformers (DCDTs) were used to monitor longitudinal inplane and out-of-plane displacements at selected locations, as shown in Fig. 2. All electrical signals and corresponding applied loads were recorded automatically at regular time intervals during the tests.

Linear Buckling Analysis

Both buckling and nonlinear postbuckling analyses were performed in this study. Linear buckling analyses were conducted for the baseline design using both PANDA2 and STAGS (Structural Analysis of General Shells[7]). Input files for the STAGS linear buckling analysis were generated by PANDA2. Next, the effect of the shear load and the geometric imperfection on the buckling loads of the baseline design were investigated using PANDA2, which employs analysis techniques with a level of fidelity similar to that of PASCO. In PANDA2, local and general buckling loads are calculated either by closed-form expressions or discretized models of panel cross sections[2,8,9] similar to those used in PASCO.

STAGS is a code for general purpose analysis of shell structures of arbitrary shape and complexity[7] with a variety of finite elements. Four-node quadrilateral plate elements with cubic lateral displacement variations (called 410- and 411-elements in STAGS) are efficient for predicting buckling response of thin shells. For plates in which transverse shear deformation is important, the assumed natural-strain, nine-node element (480-element) can be selected.[7] While the panel investigated here warrants the use of the 480-element, the 411-element was also used because the effect of shear deformation is not in the analysis for the PASCO-designed panel. STAGS results were postprocessed using PATRAN.[10]

The STAGS finite element model for the panel had a total of 20 branched shell units, and each branched shell unit had 325 nodes (for the 32-in.-long panel) or 325 nodes (for the 30-in.-long baseline design panel), respectively. The axial compressive design load (640,000 lb) was applied with a uniform end-shortening constraint along with compatibility conditions for adjacent shell unit interfaces. In the test, the load was applied to the potted ends. To simulate this boundary condition, the displacement along the z direction and rotation along the x direction were constrained at the nodal points. The adhesive film used to bond the stiffeners to the skin of the test specimen was modeled by adding a 0.0121-in.-thick isotropic layer to the model to simulate the bondline between the skin and flange. The skin middle surface was used as the reference plane in which the nodes lie, and the offset distance from the middle surfaces of the skin–flange combination was modeled as an eccentricity.

An alternative finite element modeling approach with ABAQUS[11] suggested by Greene of HKS, Inc. (private communication), was also used. In this method, instead of locating the reference plane at the midplane of the skin, the bottom plane of the blade stiffener was used as the reference plane. To include the offset distances of the midplane of skin and skin–flange combination in the model, an additional 0 deg ply with negligibly low stiffness was added to both skin and skin–flange laminates, as shown in Fig. 3. Both the nine-node thin shell element (S9R5) and the four-node general

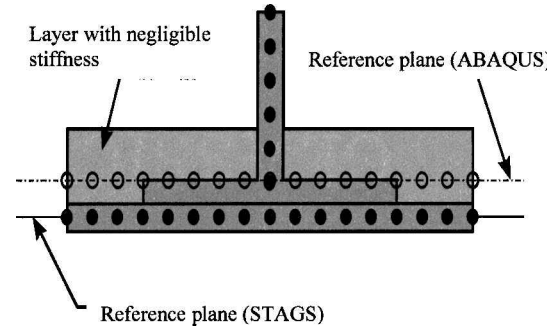

Fig. 3 Reference plane of ABAQUS and STAGS models.

shell element (S4) in ABAQUS were selected for the stiffened panel models. Both shell elements can account for transverse shear deformations and are comparable to the 480-element in STAGS. Instead of applying a compressive load at the panel end, uniform compressive displacements were applied at the nodal points along the loaded edge. To ensure a uniform state of stress along the entire panel length and to prevent bending during the prebuckling response stage, the incremental boundary condition option available in ABAQUS was chosen. The buckling load factor was computed from the sum of the reaction forces at the boundary node set.

Results of Linear Buckling Analysis

The effects of geometric imperfections, additional in-plane shear loads, boundary conditions, and material property variations on the buckling load of the stiffened panel are discussed in this section. The results are intended to help understand the effect of the assumed imperfections and the addition of in-plane shear loads on the robustness of the design.

Effect of Geometric Imperfections and Shear Load

A summary of the local buckling load factors with and without shear load, and with and without the initial bow-type geometric imperfections (±3% of the panel length) obtained from PANDA2 are presented in Table 2. The first row in Table 2 includes a comparison of PANDA2 and the STAGS (both 480- and 411-elements) for the perfect panel without a shear load. The PANDA2 results for both a Koiter-type analysis and a BOSOR4 analysis agree well with the STAGS 411-element results. The 11% difference between the results for the 480-element and the 411-element (Table 2) is suspected to be due to transverse shear deformation because the thickness of the skin–flange combination is 0.56 in. Shear deformation was not included in the original panel design, and this difference indicates that the effect is significant.

The panel with a negative (bulging in the direction of the blade) bow-type imperfection had a concave surface in the middle of the panel. Thus, the blade tip is subjected to less axial compression, and the skin is subjected to more axial compression than that of the perfect panels. Similarly, the blade tip near the boundary is subjected to more compression, and the skin near the boundary is subjected to less compression than in the perfect panel. The opposite holds true for the positive bowtype imperfection. From the last two rows of Table 2, one can note that a 3% positive imperfection results in a very low buckling load factor. The buckling load factor is reduced from 1.256 to 0.394. A 3% negative imperfection also reduces the buckling load factor (from 1.256 to 1.026), but the reduction is smaller than that for a positive imperfection. A 3% imperfection is very large for a 32-in.-long stiffened panel, and thus will lead to conservative designs.

Effects of Boundary Conditions and Material Properties

There were slight differences in material properties, panel dimensions, and boundary conditions between the baseline design and the actual test conditions. To understand the effects of these differences, analyses were conducted using both sets of input data. The differences in material properties and dimensions are summarized in Tables 3 and 4, respectively. While changes in the material properties can be input to the analyses directly, differences in the thickness of the skin or flange are accounted for by implementing a proportional change in the model's ply thickness. A detailed discussion of this procedure can be found in Ref. 4. Table 5 shows the effects of boundary conditions and material properties on the buckling load

Table 3 Material properties of baseline designs and test specimen

		E_1 (Msi)	E_2 (Msi)	G_{12} (Msi)	ν_{12}	ν_{21}
Skin	Design	18.50	1.64	0.87	0.3	0.0270
	Test specimen	17.333	1.64	0.8151	0.3	0.0284
Blade	Design	18.50	1.64	0.87	0.3	0.0270
	Test specimen	19.125	1.64	0.8994	0.3	0.0257
Flange	Design	18.50	1.64	0.87	0.3	0.0270
	Test specimen	19.593	1.64	0.9214	0.3	0.0251
Adhesive	Test specimen	0.5	0.5	0.192	0.3	0.3

Table 4 Geometric parameters of the baseline design and test specimen

Panel	Design (in.)	Test specimen (in.)
Panel length	30	32
Panel width	32	32
Blade height	3.0705	3.0723
Skin ply thickness	0.00520	0.00555
Blade ply thickness	0.00520	0.00503
Flange ply thickness	0.00520	0.00491
Adhesive thickness	0.0	0.0121

Table 5 Buckling load factors obtained from STAGS with various boundary conditions

Boundary conditions	Shell unit 480-element[a]	Shell unit 411-element
4 edges simply supported (baseline design)	1.166	1.296
2 edges free, 2 edges clamped (baseline design)	1.197	1.340
2 edges free, 2 edges clamped (potted region, test material, 32-in. panel length)	1.154	1.286

[a] Includes shear deformation.

Table 2 Summary of the local buckling load factor[a] from PANDA2 and the lowest buckling load factor from STAGS (four edges simple supported)

	PANDA2 (Koiter analysis)		PANDA2 (BOSOR4 analysis)			
Loading combination with/ without imperfection	Panel end[c]	Panel midlength[c]	Panel end[c]	Panel midlength[c]	STAGS (480-element[b])	STAGS (411-element)
$N_x = 20{,}000$ lb/in., $N_{xy} = 0$ without imperfection	1.256	1.256	1.328	1.328	1.166	1.296
$N_x = 20{,}000$ lb/in., $N_{xy} = 5{,}000$ lb/in. without imperfection	1.234	1.234	1.048	1.048	——	——
$N_x = 20{,}000$ lb/in., $N_{xy} = 5{,}000$ lb/in. with imperfection (+3%)	1.234	0.356	1.048	0.346	——	——
$N_x = 20{,}000$ lb/in., $N_{xy} = 5{,}000$ lb/in. with imperfection (−3%)	1.234	0.856	1.048	0.920	——	——
$N_x = 20{,}000$ lb/in., $N_{xy} = 0$ lb/in. with imperfection (+3%)	1.256	0.394	1.328	0.398	——	——
$N_x = 20{,}000$ lb/in., $N_{xy} = 0$ lb/in. with imperfection (−3%)	1.256	1.026	1.328	1.083	——	——

[a] Buckling occurs at the applied load times the buckling load factor. [b] Includes shear deformation.
[c] PANDA2 cannot perform exact buckling analysis under nonuniform stress field. Thus, it provides buckling loads based on the stress values near the ends and at midlength of the panel as if these represented constant stress fields.

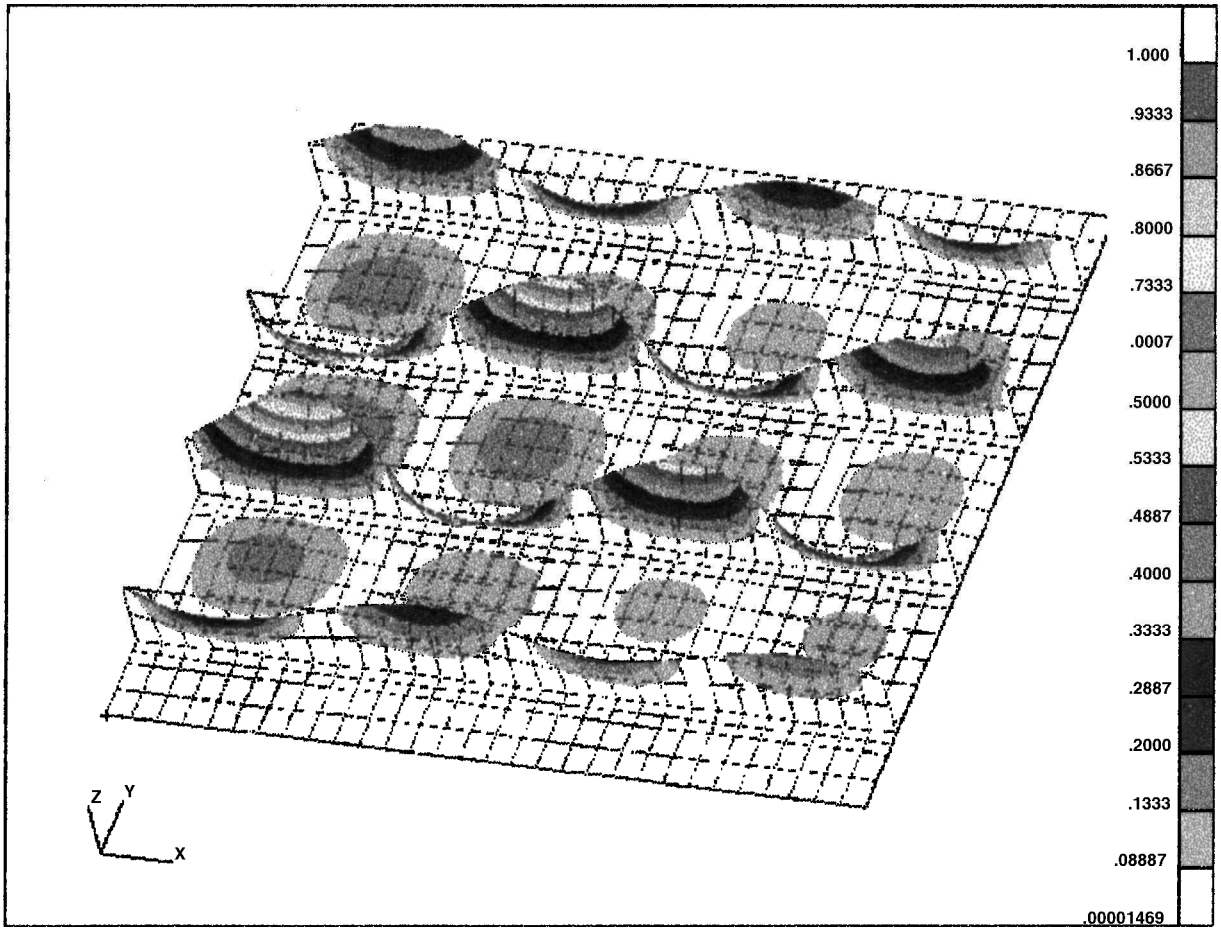

Fig. 4 STAGS-predicted buckling mode shape of the perfect baseline design panel (simply supported on four sides) subjected to uniaxial compression load (buckling load factor = 1.166).

factors. Comparison of the first two rows of Table 5 reveals that the effects of changes in the boundary conditions are not very significant. According to PANDA2 results, the lowest buckling load corresponded to local buckling, which suggests that the differences in boundary conditions between the analysis and the experiment will not have a large effect on the results. Similarly, results in the last two rows show the effects of changes in material properties and panel dimensions.

The buckling mode shape of the perfect baseline design (simply supported on four sides) predicted by the STAGS 480-element is shown in Fig. 4. The corresponding ABAQUS results are shown in Fig. 5. The overall buckling mode shape obtained from ABAQUS agrees well with that of STAGS. Both modes have four half-waves in the longitudinal directions, but even though the problem is symmetric in both directions, the buckling mode is not, as often happens. This asymmetry is more accentuated for the STAGS model, where the displacements peak not far from the support. The computed lowest buckling load factor is slightly higher than that of STAGS (1.218 for ABAQUS and 1.166 for STAGS). This small difference may be due to modeling differences discussed in the following paragraph. The STAGS prediction of the buckling mode shape of the test panel with potted boundary conditions (with the other two edges being free) is shown in Fig. 6.

An examination of the STAGS model in Fig. 3 shows that there is a double counting of the material between the blade stiffener and the flange–skin combination due to the way the nodes are located in the blade elements and in the elements that represent the flange–skin combination. These elements have midplane nodes leading to an overlap equal to the thickness of the blade with a width equal to half the thickness of the flange–skin combination. This overlap is avoided in the ABAQUS modeling approach described earlier. The additional material that results from the overlap is expected to increase the prebuckling axial stiffness of the panel. To estimate this increase, the STAGS model was modified to resemble the ABAQUS model, and a linear buckling analysis was performed on the modified model. The results of this analysis are presented in Table 6, which also compares these results with the experimental results. The increase in area due to the overlap contributed to about one-half of the difference in total stiffness between the analysis and test results.

Table 6 Comparison of prebuckling stiffness and buckling load factors (STAGS results)

	EA/L (kip/in.)	EA (kip)	Buckling load factor
Model with overlap	3931.2	125,800	1.15
Model with no overlap	3684.4	117,900	1.23
Experiment	3453.9	110,500	1.09

Summary of Differences Between Design Model and Test Model

The PASCO model used for designing the panel had several modeling simplifications and compensating factors; their effects are listed in Table 7. The two major model simplifications were as follows: 1) PASCO does not account for shear deformation, which may be significant for thick composite panels, and this effect reduces the buckling load by 11%. 2) PASCO employs simple support boundary conditions. The difference due to boundary conditions was only about 1% because the buckling mode is local.

To obtain a more robust design, the PASCO model was subjected to an additional shear load and bow-type initial imperfection with maximum amplitude of 3% of the panel length. Both of these features had substantial effects on the buckling load. However, because

Table 7 Differences between baseline design analysis and analysis of actual test panel

	Baseline design	Test panel	Effect on buckling load
Loading condition (lb/in.)			
Axial compression	20,000	20,000	
In-plane shear load	5,000	0	−20%
Imperfection (initial bow type)	−3% of panel length	Not measured	−30% (with shear load) −18% (w/out shear load)
Boundary condition			1% (with test material)
Loaded edges	Simple support	Clamped (potted)	
Unloaded edges	Simple support	Unsupported	
Transverse shear deformation	No	Yes	11%

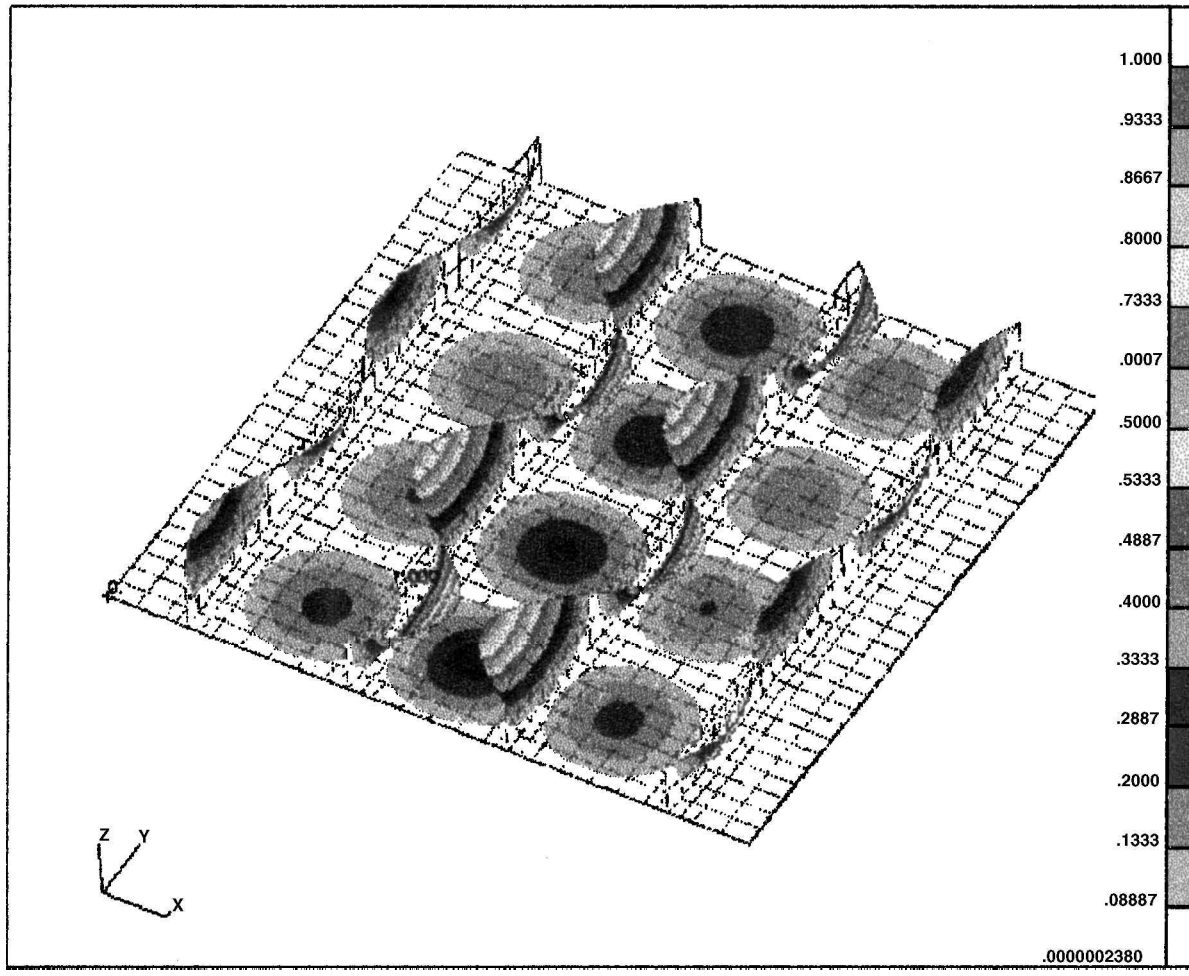

Fig. 5 Predicted buckling mode shape of the baseline design (simply supported on four sides) with nine-node shell elements from ABAQUS (bluckling load factor = 1.218).

the panel was designed only for imperfection of one sign, the design became more sensitive to an imperfection of the opposite sign. Finally, because of the substantial thickness of the blade, it was also found that a midsurface reference plane modeling, which is common in thin-walled structures, produces an approximate 7% increase in the prebuckling stiffness and a 7% reduction in buckling load. The opposite effects are explained by the fact that the stiffness of the overlap causes more load to be supported by the blade, which is the critical element. Overall, the more accurate analytical model predicts a buckling load that is about 18% higher than the design load; however, this does not take into account any initial imperfections. The actual test buckling load was only about 10% higher than the design load. For this panel, the simplified model used in PASCO, together with the shear and imperfection loading added for robustness, worked reasonably well. The other two tested designs were also within a few percent of the design load.

Nonlinear Analysis

Although the linear buckling loads provide a measure of the compressive load-carrying capacity of the stiffened panels, the test results indicate that the panels underwent substantial nonlinear transverse deformations before failure. Hence, a nonlinear analysis was performed to understand the effects of boundary conditions including the eccentricity in load application. The nonlinear analysis was performed without applying any initial imperfection, but the differences in the stacking sequence and material properties between the skin and the blades introduced small amounts of bending deformation. The modified Riks path-following algorithm in STAGS was used for the nonlinear analysis. The computation time required for the nonlinear analysis was an order of magnitude greater than that for the linear analysis, indicating significant nonlinearity with response (near the buckling load). The following subsections discuss the results of the nonlinear analyses and compare experimental and analytical results.

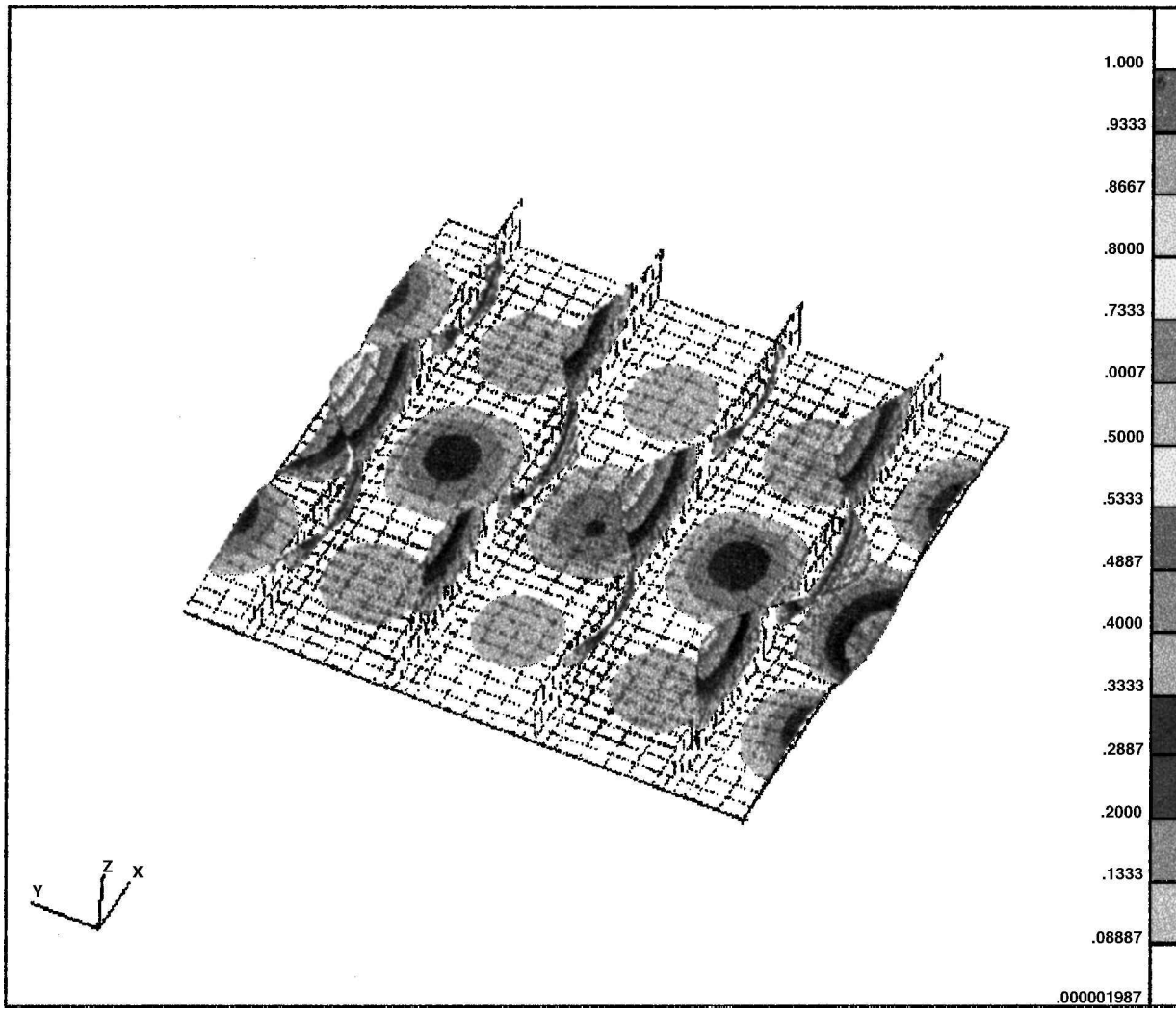

Fig. 6 Predicted buckling mode shape of the blade-stiffed panel (with test material and boundary conditions) from STAGS (buckling load factor = 1.154).

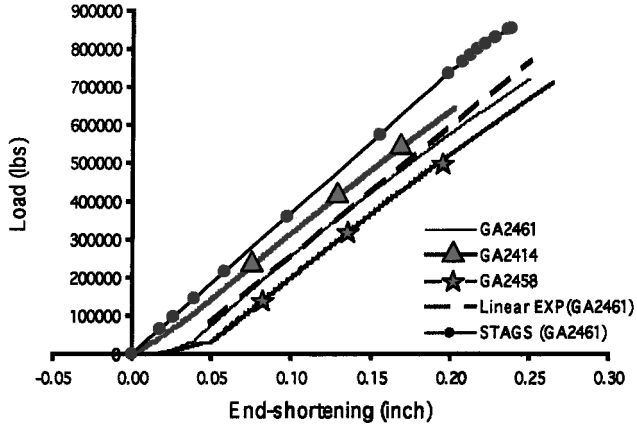

Fig. 7 Compressive load vs end shortening form analysis and experiments.

Compressive Load vs End Shortening

The compressive load vs end-shortening deflection curves from the STAGS nonlinear static analyses, the test, and a linear least squares fit of the measured data are shown in Fig. 7. The test panel designated as GA2461 in Ref. 6 is the baseline design. In addition to the baseline panel, two other test panels (GA2414, GA2458) from Ref. 6 have slightly different geometries and stacking sequences. As expected, their compressive load vs end-shortening curves from the tests exhibit a similar trend, except at the initial stage of loading. The prebuckling stiffness was calculated from the slopes of the linear portions of the experimental load vs end-shortening curves for the three panels and by multiplying the slopes by the panel length. The prebuckling stiffness from the experiments with the prebuckling stiffness predicted using STAGS for test panel GA2461 are compared in Table 8. The prebuckling stiffness of the test panels is about 6% less than that of the analysis.

Table 8 Comparison of the prebuckling stiffness and buckling load results from STAGS and experiments

	EA/L (kip/in.)	EA (kip)	Buckling load factor
STAGS nonlinear (panel GA2461)	3931.2	117,900	1.23
Experimental result (panel GA2461)	3453.9	110,500	1.09
Experimental result (panel GA2414)	3347.8	107,100	0.94
Experimental result (panel GA2458)	3333.8	106,700	1.07

Compressive Load vs Out-of-Plane Deformations

The layout of the DCDTs used to measure displacements in the test panel is shown in Fig. 2. The out-of-plane displacements, measured from DCDTs at selected locations defined in Fig. 2, are shown in Figs. 8 and 9. The results in Fig. 8 show that out-of-plane displacements were initiated at an early stage of the loading and increased

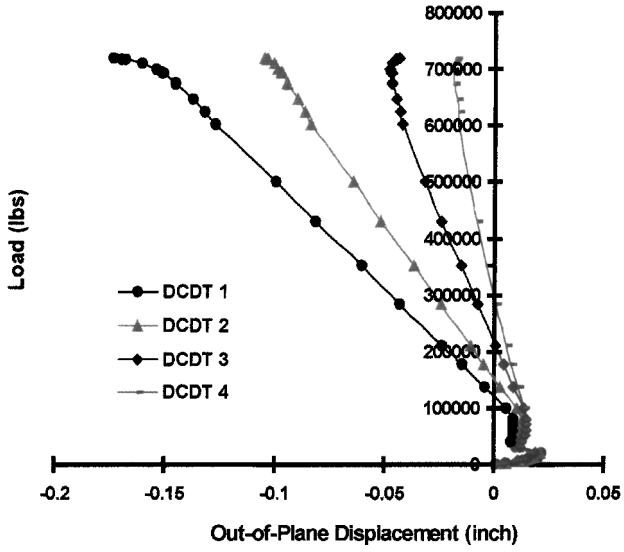

Fig. 8 Load vs out-of-plane displacements of the skin at the center bay.

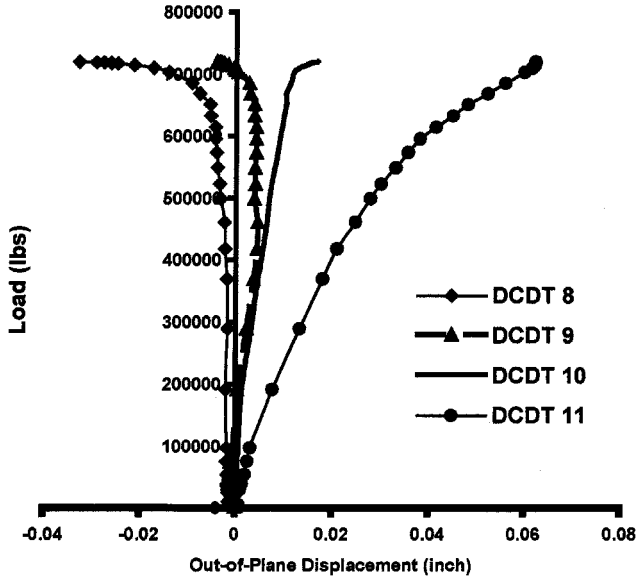

Fig. 9 Load vs out-of-plane displacements of the stiffener at selected location in Fig. 2.

linearly in proportion to the loading. Furthermore, the displacements were largest near the loaded edge. These observations suggest that loading eccentricities may exist along the load introduction edges, or rigid body rotation of the panel with respect to the clamped edge may have occurred, in addition to the effects of geometric imperfections. The results in Fig. 9 show that the out-of-plane displacements of the blade stiffeners also started at an early stage of the loading. With the exception of DCDT 11, the out-of-plane deformations were an order of magnitude lower than those of the skin in Fig. 8. Furthermore, a significant nonlinear response was only exhibited near the failure load. The large nonlinear response of DCDT 11 throughout the axial loading was probably due to the effect of the unsupported side-edge boundaries. The out-of-plane displacement variations along the length of the panel (DCDTs 1–4 in Fig. 2) at selected load levels are shown in Fig. 10. The results in Fig. 10 indicate that bending and end shortening occurred in the test panel as a result of the applied axial compression. The load vs out-of-plane displacement response across the panel at midlength can be found in Ref. 12.

To understand the substantial prebuckling bending, a combination of different geometric imperfections and loads applied at small angles to the axial direction as analyzed to determine their influence on

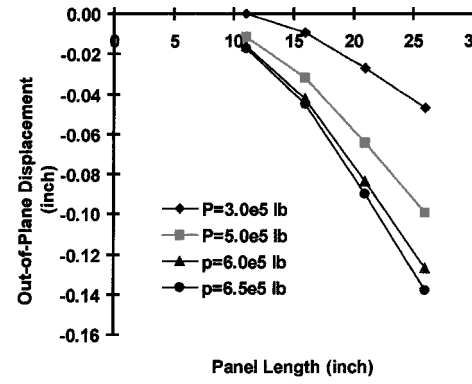

Fig. 10 Variation of the out-of-plane displacements along the panel lengthwise direction.

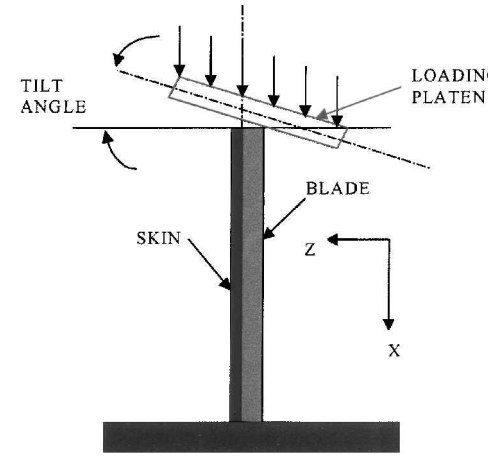

Fig. 11 Schematic of blade-stiffened panel and loading platen.

the observed out-of-plane displacements. Geometric imperfections in the shape of the buckling modes were modeled in STAGS. Various combinations of imperfection amplitudes and load angles were considered. Although for some combinations it was only possible to partially reproduce the test results,[12] obtaining the right imperfection and load introduction angle seemed elusive. This difficulty suggests that the source of the prebuckling bending response was caused by some other effects.

Contact Between the Panel and Loading Platen

Hilburger[13] investigated the effects of nonuniform load introduction and boundary condition imperfections on the compression response of composite cylindrical shells with cutouts. He defined the nonuniform load distribution as being other than a uniform axial displacement of the cylinder's loading surface and found two sources of nonuniform load introduction. One source was due to lack of planarity in the loading surfaces of the specimen and the loading platens. The other source was due to tilting of the loading platen with respect to the specimen before the loading began. Hilburger measured the top and bottom loading surface imperfections as well as the potting thickness. These imperfection data were fitted to curves and input into STAGS models. Furthermore, the test frame loading platen was modeled as rigid flat plates, and STAGS generalized contact analysis was used. (Generalized contact definition means that contact points are calculated by STAGS rather than specified by the user.)

A similar modeling approach was used in the present study to identify the causes of the substantial out-of-plane deformations and nonlinear end shortening during the early stage of the test. The loading platen was modeled as a rigid flat plate in the STAGS analyses. Because the loading surface imperfections were not measured before the test, they were not considered in this study. Instead, it was assumed that the rigid loading platen initially contacted at the tip of the blade stiffeners at a small tilt angle, as shown in Fig. 11.

Table 9 Summary of contact angles and stiffnesses of contact element

	Panel length (in.)	Contact angle (deg)	Force–displacement relation for contact element[a] (lb/in.)					
Model 7	30	0.01	Disp.	0.005	0.05	0.1	0.2	1.0
			Force	1.0e3	1.0e5	1.0e7	2.0e8	2.0e8
Model 8	30	0.01	Disp.	0.0001	0.03	0.05	0.2	1.0
			Force	1.0e3	1.0e7	1.0e8	2.0e8	2.0e8
Model 9	30	0.01	Disp.	0.005	0.03	0.05	0.2	1.0
			Force	1.0e3	1.0e5	1.0e8	2.0e8	2.0e8
Model 10	30	0.005	Disp.	0.005	0.03	0.05	0.2	1.0
			Force	1.0e3	1.0e5	1.0e8	2.0e8	2.0e8

[a] STAGS interpolates for intermediate values.

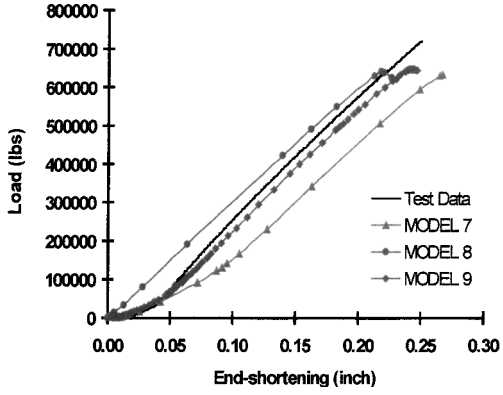

Fig. 12 Compressive load vs end shortening from analyses with contact models and experiment. Model numbers refer to Table 9.

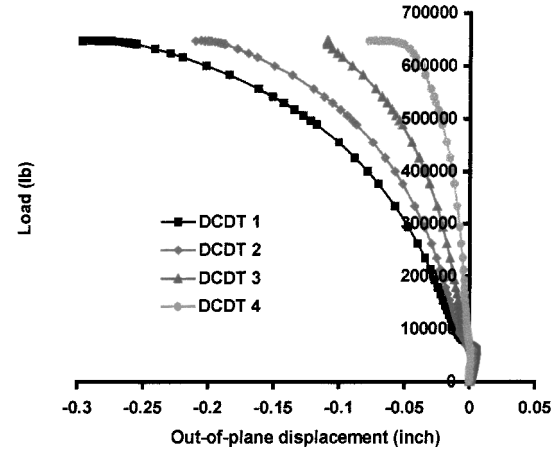

Fig. 13 Load vs out-of-plane displacements of the skin at the center-bay, from the analysis result (model 9).

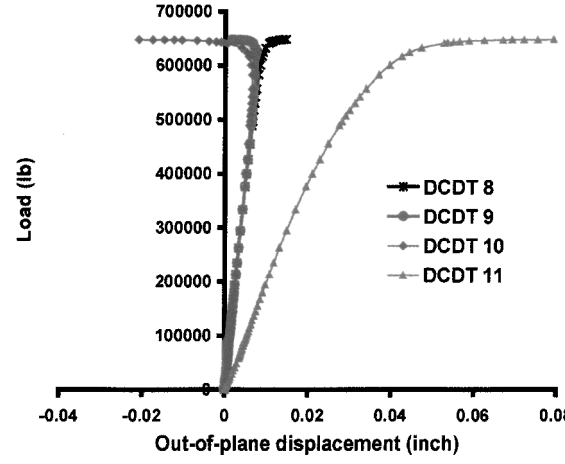

Fig. 14 Load vs out-of-plane displacements of the stiffeners at selected locations, from the analysis result (model 9).

The panel in Fig. 11 is shown sideways, with the bottom element representing the bottom support of the loading aparatus.

As the analysis progresses, STAGS uses generalized contact analyses to check for contact and to construct contact element-coupling contact points with the contacted shell elements. In doing this, STAGS uses penalty functions to enforce displacement compatibility between each contacting point and each element with which it is in contact. STAGS utilizes analyst-supplied stiffness vs displacement information to compute the forces that may result from the small contact-surface penetration. A contact element is conceptually a nonlinear spring connecting the contact point to the surface of the contacted element. This nonlinear spring typically has low stiffness when the contact-surface penetration is small, but it gets progressively stiffer as penetration increases.[7]

Generalized contact analyses were implemented for the finite elements that simulate the rigid platen and load introduction edge of the test specimen. The selection of proper stiffnesses of the contact elements for the present analyses is somewhat arbitrary. Therefore, several nonlinear analyses were performed to simulate the observed out-of-plane deformation response of the test specimen by changing both the tilt angles and the stiffnesses of the contact elements between the loading platen and load introduction edge. The combinations of the tilt angles and stiffnesses of the contact elements used for the analyses are summarized in Table 9, and the corresponding load vs end-shortening results are shown in Fig. 12. The results in Fig. 12 suggest that the computed end-shortening responses strongly depend on the user-supplied input data in Table 9. Among the computed load vs end-shortening responses, the response of model 9 is quite similar to that of the test panel in Fig. 12. The computed out-of-plane displacements of the skin and stiffeners of model 9 at the selected DCDTs locations are further indicated as shown in Figs. 13 and 14, respectively. The response of model 9 in Fig. 13 shows a good correlation with those of the test panel skin in Fig. 8 during the early stages of the load history. However, model 9 exhibits a considerable nonlinear out-of-plane deformation of the skin when the compressive load is above 400,000 lbs. This was not present in the results for the response of the test panel in Fig. 8.

Generalized contact analyses revealed that the panel was locally buckled at about 80,000 lb. The global buckling occurred at load level 650,000 lb (load factor of 1.016), where significant nonlinear out-of-plane deformations were seen, as shown in Fig. 13. This compares to a load factor of 1.23 from the nonlinear analysis without the contact analysis and 1.09 from the experiment (see Table 8). The computed load vs out-of-plane stiffener deformation at DCDT 11 has significant nonlinear behavior, as shown in Fig. 14. This significant nonlinear response was also observed from the measured response of the actual test panel, as shown in Fig. 9. In general, the finite element model with the generalized contact analyses improved correlation between the measured and predicted out-of-plane deformation. However, the details of the displacements are considerably different. Some combination of tilt angles and contact stiffnesses can produce the observed pattern, but there may be some other causes that affect the out-of-plane displacements.

Conclusions

Computational cost considerations often dictate the use of simplified models in structural design optimization. The effect of such simplifications was examined by analyzing test results and finite element simulations for a stiffened composite panel designed with a simple finite strip model.

Several structural analysis models were used to assess the adequacy of the design model and the correlation with experimental results. Shear deformation was the most important of the effects neglected by the simple model, accounting for about 11% difference in buckling load. The effect of simplified (simple support) boundary conditions was small. The addition of shear loads and initial imperfections to the design model improved the correlation of the results, even though including an imperfection that was biased in one direction apparently induced an increased sensitivity to imperfection in the other direction. Overall, the simplified model produced designs that failed within 10% of the design load in the experiments.

The most significant difference between the analytical predictions and the experimental measurements was the substantial out-of-plane prebuckling deformations. To explain these differences, imperfections, load eccentricities, and loading platen tilt angles were considered. Of these, the loading platen tilt produced patterns of deformation similar to the measured deformations but with more nonlinear characteristics.

Acknowledgments

This work was supported in part by NASA Langley Research Center under Grants NAG1-2000 and NAG1-2177. The authors wish to acknowledge the generous help provided by David Bushnell, the developer of PANDA2, William Greene of HKS, Inc., and Mark Hilburger of NASA Langley Research Center. The authors also wish to express their appreciation to Allen Waters of NASA Langley Research Center, who provided the experimental data.

References

[1] Stroud, W. J., and Anderson, M. S., "PASCO: Structural Panel Analysis and Sizing Code, Capability and Analytical Foundations," NASA TM-80181, 1981.

[2] Bushnell, D., "PANDA2-Program for Minimum Weight Design of Stiffened, Composite, Locally Buckled Panels," *Computers and Structures*, Vol. 25, No. 4, 1987, pp. 469–605.

[3] Nagendra, S., Haftka, R. T., Gürdal, Z., and Starnes, J. H., Jr., "Design of Stiffened Composite Panels with a Hole," *Composite Structures*, Vol. 18, 1991, pp. 195–219.

[4] Whetstone, J. D., *EISI-EAL Engineering Language Reference Manual*, EISI-EAL System Level 2091, Engineering Information Systems Inc., Saratoga, CA, July 1983.

[5] Nagendra, S., Haftka, R. T., Gürdal, Z., and Starnes, J. H., Jr., "Buckling and Failure Characteristics of Compression-Loaded Stiffened Composite Panels with a hole," *Composite Structures*, Vol. 28, 1994, pp. 1–17.

[6] Nagendra, S., Jestin, D., Gürdal, Z., Haftka, R. T., and Watson, L. T., "Improved Genetic Algorithm for the Design of Stiffened Composite Panels," *Computers and Structures*, Vol. 58, No. 3, 1996, pp. 543–555.

[7] Brogan, F. A., Rankin, C. C., and Cabiness, H. D., *STAGS Users Manual*, LMSC P032594, Version 2.0, Lockheed Palo Alto Research Lab., Palo Alto, CA, June 1995.

[8] Bushnell, D., "Optimization of Composite, Stiffened, Imperfect Panels Under Combined Loads for Service in the Postbuckling Regime," *Computer Methods in Applied Mechanics and Engineering*, Vol. 103, 1993, pp. 43–114.

[9] Bushnell, D., and Bushnell, W. D., "Minimum-Weight Design of a Stiffened Panel via PANDA2 and Evaluation of the Optimized Panel via STAGS," *Computers and Structures*, Vol. 50, No. 4, 1994, pp. 569–602.

[10] Anon., "P3/PATRAN User Manual," The MacNeal-Schwendler Co., Los Angeles, CA, May 1995.

[11] *ABAQUS/Standard User's Manual*, Hibbit, Karlsson & Sorensen, Inc. 1996.

[12] Park, O., Haftka, R. T., Sankar, B. V., and Nagendra, S., "Analytical and Experimental Study of a Blade Stiffened Panel in Axial Compression," AIAA Paper 98-1993, April 1998.

[13] Hilburger, M. W., 'Numerical and Experimental Study of the Compression Response of Composite Cylindrical Shells with Cutouts," Ph.D. Dissertation, Aerospace Engineering Dept., Univ. of Michigan, 1998.